SCIENTIFIC REPORTS

OPEN

SUBJECT AREAS:
MECHANICAL PROPERTIES
CHEMICAL PHYSICS
MECHANICAL AND STRUCTURAL PROPERTIES AND DEVICES

Received
10 October 2013

Accepted
5 March 2014

Published
24 March 2014

Correspondence and requests for materials should be addressed to J.-H.A. (ahnj@yonsei.ac.kr) or S.-M.L. (sm.lee@kimm.re.kr)

* These authors contributed equally to this work.

Fracture Characteristics of Monolayer CVD-Graphene

Yun Hwangbo[1]*, Choong-Kwang Lee[2]*, Sang-Min Kim[1], Jae-Hyun Kim[1,3], Kwang-Seop Kim[1], Bongkyun Jang[1], Hak-Joo Lee[1], Seoung-Ki Lee[4], Seong-Su Kim[2], Jong-Hyun Ahn[4] & Seung-Mo Lee[1,3]

[1]Department of Nanomechanics, Nano-Convergence Mechanical Systems Research Division, Korea Institute of Machinery & Materials (KIMM), 156 Gajungbuk-ro, Yuseong-gu, Daejeon, 305-343, South Korea, [2]Department of Organic Materials & Fiber Engineering, Chonbuk National University, Jeonju, 561-756, South Korea, [3]Nano Mechatronics, University of Science and Technology (UST), 217 Gajeong-ro, Yuseong-gu, Daejeon 305-333, South Korea, [4]School of Electrical and Electronic Engineering, Yonsei University, Seoul, 120-749, South Korea.

We have observed and analyzed the fracture characteristics of the monolayer CVD-graphene using pressure bulge testing setup. The monolayer CVD-graphene has appeared to undergo environmentally assisted subcritical crack growth in room condition, i.e. stress corrosion cracking arising from the adsorption of water vapor on the graphene and the subsequent chemical reactions. The crack propagation in graphene has appeared to be able to be reasonably tamed by adjusting applied humidity and stress. The fracture toughness, describing the ability of a material containing inherent flaws to resist catastrophic failure, of the CVD-graphene has turned out to be exceptionally high, as compared to other carbon based 3D materials. These results imply that the CVD-graphene could be an ideal candidate as a structural material notwithstanding environmental susceptibility. In addition, the measurements reported here suggest that specific non-continuum fracture behaviors occurring in 2D monoatomic structures can be macroscopically well visualized and characterized.

In fracture mechanics, the term, stress intensity factor (SIF, K) emerged from Griffith's concept[1] and Irwin's modification[2], has been used to determine the fracture toughness (K_{Ic}) which is widely accepted as a yardstick describing the ability of a material containing inherent flaws to resist catastrophic failure. Unlike bulk 3D materials intensively studied so far, fracture characteristics of the 2D material have remained nearly undisclosed. Lately, the graphene, carbon based ideal 2D material, discovered in 2004[3] has sparked massive movement to dig the secret of 2D physics open[4,5]. Although the basic mechanical properties of the 2D materials, graphene, have been hitherto theoretically predicted from the viewpoint of defect physics[6–12] and experimentally measured[13–16], even till now, the specific fracture behaviors, particularly, fracture toughness, have remained largely unknown, and even worse, experimental results are quite rare. Here we probed the fracture behaviors of the monolayer graphene grown by chemical vapor deposition (CVD) using a pressure bulge tester equipped with real time cinematography system. The CVD-graphene appeared to show environmentally assisted subcritical crack growth behavior, which is believed to result primarily from the combined effect of the mechanical stress and environmental conditions, i.e. stress-enhanced chemical reactions between graphene and water molecules in air (stress corrosion cracking). The by-product of the wet transfer, i.e., polymethylmethacrylate (PMMA) residue existing on the transferred CVD-graphene, has turned out to have minor effect on general fracture behavior of the graphene despite its moisture absorption property. To astonishment, the propagation of cracks in the graphene has appeared to be able to be reasonably tamed by adjusting applied humidity and stress. The fracture toughness of the CVD-graphene has turned out to be exceptionally high (10.7 ± 3.3 MPa $m^{1/2}$), as compared to other carbon based 3D materials. This high fracture toughness suggests that the CVD-graphene could be an ideal candidate as a structural material notwithstanding environmental susceptibility.

Results

Suspended graphene membrane: preparation and characterization. For the preparation of the suspended graphene membrane on arbitrary substrate suitable for the pressure bulge test and the real time cinematography, firstly, graphene grown by the CVD on polycrystalline copper (Cu) was transferred onto SiO_2 substrate with a cylindrical hole ($10 \sim 110$ μm diameter) utilizing the PMMA based transfer method (Fig. 1a, and Fig. S1 in Supplementary Information). For this experiment, a large number of samples (graphene/SiO_2/Si)

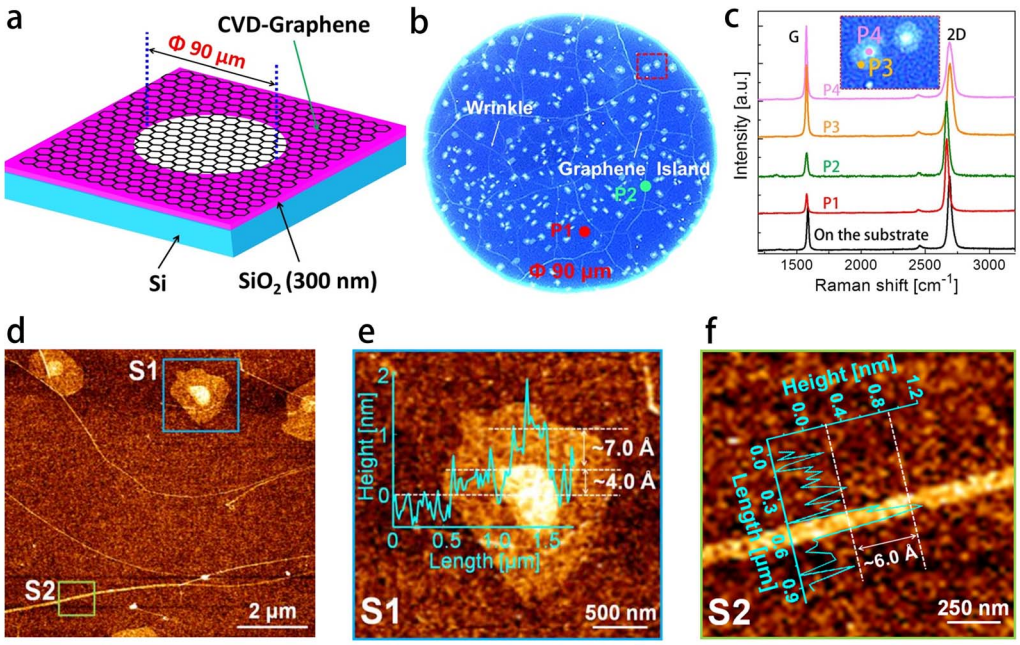

Figure 1 | Preparation and characterizations of the suspended CVD-graphene membrane. (a), Schematic of the freely suspended CVD-graphene on SiO_2 substrate with a cylindrical hole. (b), Optical microscope image of the suspended monolayer graphene with wrinkles and graphene islands. (c), Comparison of Raman spectra (excitation wavelength $\lambda = 514$ nm) measured on various locations, P1: monolayer graphene, P2: wrinkle, P3 and P4: graphene island. (d–f), Contact mode AFM images of the graphene with wrinkles and islands, which were measured at the supported graphene on Si substrate near the suspended graphene.

with various hole sizes were initially prepared. Per sample, bulge test together with detailed analyses were carefully carried out one by one, and at the same time whole fracture processes were filmed with a high speed or CCD (charge coupled device) camera (See Materials and Method in SI). In the following, we demonstrated the representative results obtained from CVD-graphene suspended on a hole with a diameter of 90 μm (Table S1).

The prepared graphene membrane (90 μm diameter) was carefully examined with an optical microscope in order to confirm whether the graphene is safely suspended on Si substrate because the membrane is often ripped due to the unavoidable mechanical stress developed during wet etching and drying in air (Fig. S2). By adjusting the illumination intensity of the optical microscope, the presence of the wrinkles generated by the different thermal expansion coefficients of the graphene and the Cu catalyst[17], and the graphene islands likely formed by heterogeneous nucleation at defects such as step bunches and impurities on Cu surface[18,19], were legibly identified (Fig. 1b and Fig. S3). The thickness information of the suspended monolayer graphene was confirmed with Raman spectroscopy (Fig. 1c and Table S2)[20]. The doping effect by dangling bonds on SiO_2 substrate[21,22] and strain effect due to surface roughness of SiO_2 substrate could influence the graphene, thereby giving rise to relative Raman peak shifts. The red shifts of the G and 2D bands varying with locations (P1–P4 in Fig. 1c) are likely stemmed from biaxial straining effects (Supplementary Discussion **I**)[23]. Namely, when the graphene membrane was transferred onto target substrate and dried in air for the sample preparation, the membrane is thought to be adhered to the vertical wall of the hole presumably because of van der Waals attraction to the Si substrate, thereby inducing biaxial tension. The intensity ratio (I_{2D}/I_G) on the wrinkles (P2) and islands (P3, P4) were measured to be much smaller than on the rest of membrane (P1), which indicates that these regions are composed of multilayered graphene, as further verified by atomic force microscope (AFM) imaging (Fig. 1d–f). Among the various folding structures of the graphene, the islands (S1) and wrinkles (S2) observed in our sample were turned out to be mainly double layered islands[18] and doubly folded wrinkles[17], respectively, considering measured thicknesses on several locations.

Fracture behaviors: crack arresting and bifurcation. For characterizing the fracture behavior of the monolayer CVD-graphene, the prepared sample (Fig. 1) was mounted on the bulge test apparatus equipped with a synchronized high speed camera, as depicted in Fig. 2a. Gradually increasing pressure difference, $\Delta P = P_{atm} - P_i$, in room conditions ($T = 20^{\circ}C$ and relative humidity (φ) = 35%), we monitored crack initiation and propagation. Concurrently, the whole processes were recorded with the high speed camera (500 fps) and later on adapted for a slow-motion picture (Fig. S4 and Movie S1). For the satisfactory resolution of the observed cracks, the illumination adjustment was required depending on the surface conditions of the samples to be tested. Some poorly prepared graphene samples were observed to burst or crack immediately after applying pressure. In those samples, cracks were mainly initiated at the edge. We were able to apply differential pressures of 1.5 ~ 2 kPa to the well-prepared samples when the hole diameter was 90 μm. In those pressure ranges, the minimum sized cracks on the CVD-graphene membranes identifiable by optical microscope first appeared. As for the path of the running crack, it was unable to readily identify the crack edge although the crack was reported to propagate straight along zigzag or armchair directions with occasional change of the direction[16]. Given that the CVD-graphene has topological lattice defects like vacancies and Stone-Wales defects (a combination of two pentagon-heptagon pairs)[15], it is considered that the crack initiates at the grain boundaries and propagates along the boundaries (intergranular) or deflects into a grain (transgranular) depending on environmental conditions (Supplementary Discussion **II**)[10]. Besides, diversely sized pinholes likely generated by inter-domain merging taken placed on the CVD growth or by transferring graphene onto Si substrate are also believed to be another feasible crack initiation source. The diversely shaped pinholes (circular or elliptical) naturally have different stress concentration factors (stress singularity), which would be an

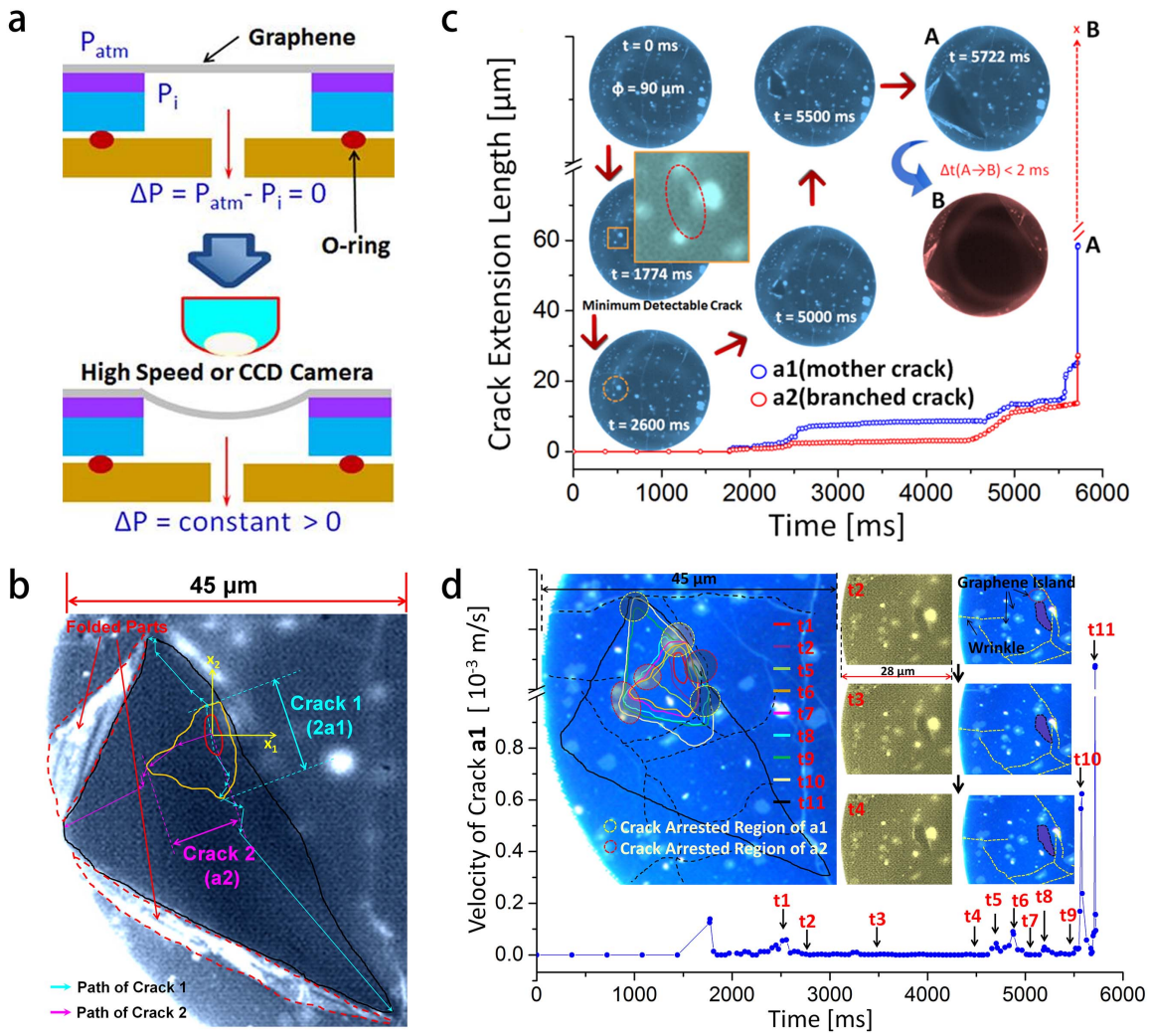

Figure 2 | Fracture behaviors of the CVD-graphene under static load condition. (a), Schematic illustration of the bulge test of the freely suspended CVD-graphene on Si substrate with a cylindrical hole. (b), One exemplified image for precisely measuring the crack extension length of the mother crack (a1) and the branched crack (a2). (c), Crack extension histories of the mother/branched crack with typical images showing fracture evolution. (d), Propagation speed diagram of the mother crack and crack arresting behaviors arising out of thickness differences (See the text). The growth rate of the branched crack can be found in Fig. S8.

important factor to determine whether or not the crack propagates. The flaw with sharper geometry would have a higher probability to further propagate due to the higher stress concentration factor (Fig. S5).

Because, during the bulge test, the static pressure differences were maintained and rapidly adjusted by a feedback controller, the pressure differences occurred during crack extension was able to be assumed to be nearly constant, i.e., quasistatic loading condition. A wealth of data on the crack evolution was provided from the recorded film (over 3000 pictures), which was examined frame by frame and around 120 representative pictures were processed for demonstration. The crack lengths were directly measured with care using the built-in software of the optical microscope (Fig. 2b and Figs. S6–S7). Figure 2c shows crack extension histories of the CVD-graphene when the applied pressure (ΔP) was 1.5 kPa. After appearance of the minimum detectable crack, the crack grew in a discontinuous and complicated manner, which was followed by the catastrophic failure of the CVD-graphene within a time of less than 2 ms (A → B). Interestingly, the growth proceeded as a succession of crack arrest and re-initiation similar to the behavior frequently observed in 3D bulk materials. The plateaus of the extension history curves alluded to the presence of the crack arresting, which could be further substantiated from velocity variation curves. As shown in Fig. 2d, the crack growth rate is shown to drop to nearly zero upon crack arresting. For instance, from t2 to t4, the crack does not propagate and the corresponding captured images are also showing hardly perceivable variations in crack length extension. Because the graphene consists of a uniform carbon based 2D monolayer, the retardation of the propagating crack by certain growth inhibitor could be intuitively regarded as a less probable phenomenon. The inhibitor, however, was revealed to be the thick graphene islands and wrinkles existing on the CVD-graphene, as can be recognized from Fig. 2d and Fig. S8. Namely, the thickness difference leads to substantial resistance to the propagation of the crack, which in turn acts as crack arresters, thereby preventing abrupt crack propagation and extending lifetime of the CVD-graphene.

As another noteworthy feature, along with the propagating main crack (a1), the bifurcated crack (branched crack, a2) instantaneously started to grow in a similar manner to the crack branching generally observed in 3D bulk crystalline materials. The branching phenomenon in the bulk materials has been believed to result from the dynamic instability of the single propagating crack, which occurs when the crack speed exceeds a certain critical velocity described as a fraction of Rayleigh wave speed[24]. The crack branching occurred

in the CVD-graphene, however, is considered to be not the case. Considering the hitherto revealed fact that the CVD-graphene is composed of polycrystalline structure containing numerous defects, which can surely offer not only preferential interaction sites between diverse absorbates and graphene[25], but also likely chemical doping sites[26,27], the macroscopic crack branching observed here is thought to arise from environmentally assisted inter- or transgranular stress corrosion crack propagation, i.e. stress corrosion crack branching[28–30] rather than the dynamic instability (Supplementary Discussion **III**). Our deduction of the stress corrosion cracking was able to be elucidated from the typical trimodal behavior observed in the diagram ($V-K$ plot) of the relation between SIF (K) and the crack velocity (V) in the CVD-graphene (Figs. 3 and S9). The detailed calculation procedures of SIF can be found in Supplementary Discussion **IV**.

Environmentally assisted cracking and fracture toughness. The interpolated curve in Fig. 3 revealed a similar shape of the typical SIF versus crack velocity (or crack growth rate) ($V-K$) diagram with trimodal region generally observed in subcritical crack growth behavior, especially, stress corrosion cracking. Crack arresting leads to decrease of the crack velocity in the diagram. The data points related to the crack arresting are marked with open red or blue squares. Those points were excluded for the interpolation since the crack arresting is not universal behaviors occurred on the whole monolayer, but just local phenomenon caused by the thickness differences. Theoretical calculation predicted that the fracture toughness of the graphene is around 3.7–6.0 MPa $m^{1/2}$ [6,8]. Contrary to the theoretical values, our experimental results revealed that the fracture toughness of the CVD-graphene is slightly higher (10.7 ± 3.3 MPa $m^{1/2}$). Taking into account the fact that polycrystalline materials could have much higher fracture toughness than the single crystalline materials due to the crack deflection[31], this divergence is likely caused by the differences in crystallinity. Unlike the single phase polycrystalline CVD-graphene with numerous grains and grain boundaries, the models of graphene adopted in theoretical calculations are mostly defect free, i.e. a single grain. In addition, it was beyond expectation that the CVD-graphene has superior fracture resistance to other pure carbon materials (like, graphite and diamond) as well as widely-used polymers and ceramics (see Table S3). Another distinctive centerpiece was that the CVD-graphene is neither overly brittle nor utterly ductile in terms of the measured fracture toughness values, although the toughness value was far below the values of ductile materials with metallic bonds. In other words, against the expected brittleness of the CVD-graphene caused by covalent bonds, it rather exhibited less brittle nature. Furthermore, the fracture toughness value was found to be close to the values of the biomaterials with hierarchically well-defined micro/nano structures like wood, and composites obeying the rule of mixtures like steel reinforced concrete. Making allowance for the variability of the configuration factor (i.e. $Y > 1$, see Fig. S10) and the neglected residual tension for the calculation ($\sigma_0 \neq 0$), the actual K_{Ic} value of the CVD-graphene is thought to be relatively higher than the obtained value in this work. Specifically, as can be recognized from the Raman shifts of the suspended CVD-graphene (Fig. 1c and Table S2), the position of 2D band showed large redshift. It clearly intimates that the suspended graphene is subjected to tension ($\sigma_0 > 0$)[32], which naturally results in higher K_{Ic} (i.e. $K_{I,a} = (\sigma + \sigma_0) Y \sqrt{\pi a}$).

The trimodal cracking-motion behavior (region **I**, **II** and **III** in Fig. 3) of the CVD-graphene under quasistatic load was believed to be intimately related to the stress-enhanced chemical reaction between molecules in atmosphere, particularly, H_2O and C-C bonds of the graphene, which presumably occurs dominantly at the crack tip where the stress is high. Our inference related to the causative role of the stress corrosion in the fracture behavior of the CVD-graphene becomes more plausible, considering the fractures of the CVD-graphene from unknown cause which have been frequently observed so far during our experiments. Namely, the initially fully covered and well suspended CVD-graphene membranes on the Si substrate with a cylindrical hole have been observed to start fracturing in a few days or

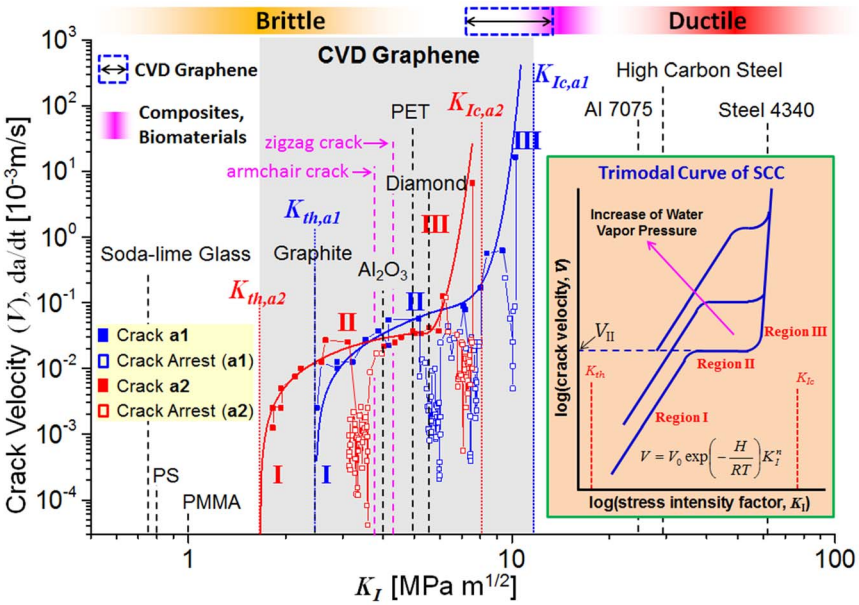

Figure 3 | Stress intensity factor (K_I) versus crack velocity (or growth rate, $V = da/dt$) diagram for the CVD-graphene in room conditions. The details of the calculation procedures are described in Supplementary Discussion **IV**. Comparison of the measured or calculated facture toughness (K_{Ic}) values between the CVD-graphene and the widely-known materials are summarized with proper references in Table S3. The data points marked with an open square (blue or red colored) denote ($V-K_I$ values associated with crack arresting, which were excluded for the interpolation (See the text for the details). The inset shows typical trimodal curve of stress corrosion cracking, which was redrawn making reference to the previous report[28]. The detailed description can be found in Fig. S9.

even in a few hours after keeping it under the relative humidity of 95%, whereas the graphene membranes kept under the relative humidity of 15% have shown negligible fracturing even after a few days, as described in Fig. 4a. Diverse fracture patterns have been observed till now. Most of the fractured graphene membranes have shown the state that the propagating crack is arrested by the graphene wrinkles or islands (Fig. S11).

Effects of PMMA residues on graphene. As another notable concern, one may wonder whether the calculated fracture toughness and the observed stress corrosion cracking behavior of the graphene was presumably influenced by the PMMA residues, because the graphene membranes used in this research were prepared by PMMA-based wet transfer method. Moreover, it has been widely accepted that the PMMA residue in the form of continuous film with thickness of 1 ~ 2 nm or uneven film could be formed on the graphene even after the PMMA is removed with acetone, and the graphene's property is influenced by the residue[33]. In order to clarify this issue, AFM investigation was performed, which showed that, on the graphene membranes used in the bulge test, the PMMA residues exist in the form of island shape, not continuous film, and the bonding strength between the residue and the graphene is rather weak (Fig. S12). Besides, it was found that thermal annealing can markedly reduce distribution density of the residue islands. In some cases, the residues would be able to lead to erroneous measurement of fracture toughness as well as other material properties, such as stiffness (E) and fracture strain (ε_f). However, the effect of the residue on fracture toughness is thought to be quite minor even in case the graphene is covered with the residue, considering a design strategy of hybrid materials. Namely, any two materials can, in principle, be combined to make a new composite. However, synergetic toughness enhancement of the PMMA islands/graphene structure can be hardly expected unless the layers are fully dense and strongly bonded[34]. Given that the graphene used is weakly covered with the residue islands and the K_{Ic} of PMMA is incomparably low (1 MPa $m^{1/2}$ at the most), it is unlikely that the residues have serious effects on the general fracture behavior of the CVD-graphene. In particular, the fracture toughness would be almost invariant, although the crack propagation path would be partly influenced since the thick residue islands could function as crack arrestors.

Tamed cracks in graphene. Although the fracture toughness of the graphene could remain largely unaffected by the existence of the PMMA residue islands, the crack initiation/propagation in graphene would be influenced. Namely, because PMMA easily absorbs moisture in air, the PMMA residue may function as local moisture (water) reservoirs when the graphene with residues undergoes stress corrosion cracking. Thus, it can be assumed that the crack in graphene could be initiated and propagated by adjusting the density of the existing PMMA residues or relative humidity and the magnitude of the applied stress. In order to substantiate this assumption, a humidity chamber was set up, in which the applied pressure (ΔP) and the relative humidity (φ) could be intentionally adjusted (Fig. 4B). Instead of the unannealed CVD-graphene, the thermally annealed CVD-graphene (250°C, 2 h) with the markedly reduced PMMA residues have been used in bulge test. As described in the profile of $\Delta P/\varphi$ vs time (t) in Fig. 4B, starting from the state 1 ($S1$), i.e. $S1(\Delta P, \varphi) = S1$ (0 kPa, 20%), pressure and humidity were adjusted and at the same time all images were sequentially recorded with CCD camera. Firstly, the pressure was increased under constant humidity ($S2$) and concurrently the graphene was carefully inspected down to the minute details. As can be easily noticed from the time scale in the graph, for long duration from $S2$ to $S3$, any evident change was not detected. However, it was clearly observed that, at constant pressure, the humidity is no sooner increased than the crack is initiated [$S3$(11 kPa, 20%) → $S4$(11 kPa, 60%)]. Subsequently, the initiated crack was observed to continuously undergo subcritical crack growth (from $S3$ to $S4$) and eventually lead to catastrophic failure ($S5$). Similar control experiments were repeated with other samples under different pressure/humidity combinations. It clearly appeared that the crack in the CVD-graphene can be initiated by humidity and undergoes subcritical crack growth, although the applied pressure also has certain effects (Figs. S13–S14). A noteworthy difference in fracture behavior between the thermally

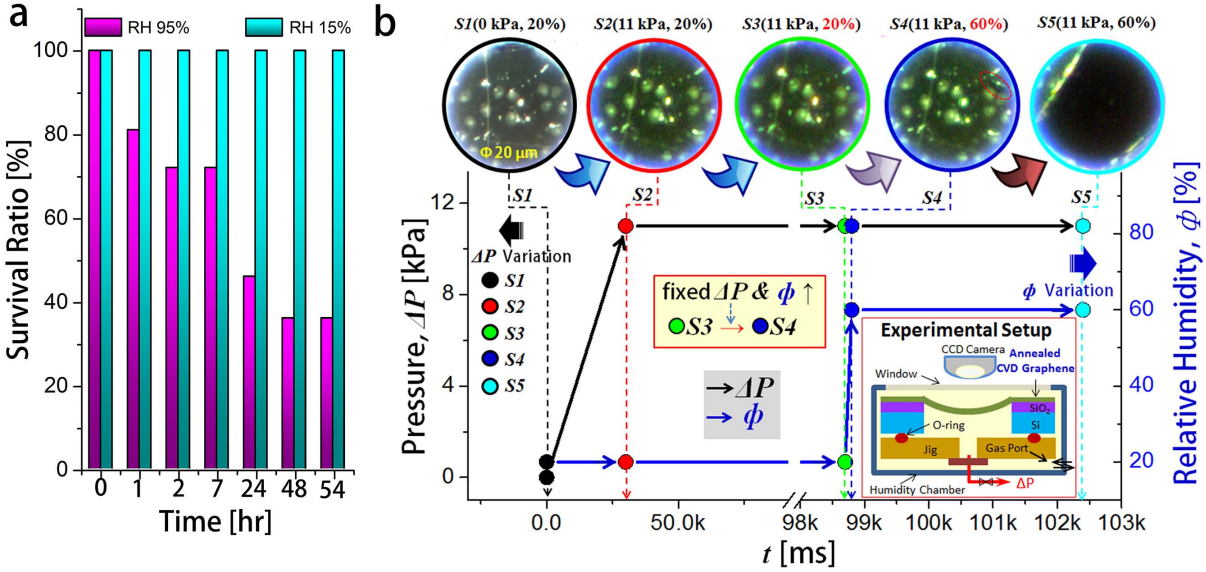

Figure 4 | Evidence for the reactions between water and CVD-graphene. (a), Dozens of the CVD-graphene membrane samples suspended on a hole (diameter: 90 μm) were separately kept in isothermal-isohumidity chamber with the relative humidity of 95% and 15%, respectively. Every hour, the samples were taken out and examined using the optical microscope whether the membranes are broken or not. By counting the number of the broken/unbroken samples, the survival ratios were calculated. (b), Fracture behavior of the thermally annealed CVD-graphene under the condition of varying humidity and fixed pressure. The inset shows schematic description of the used humidity chamber and bulge test setup. The humidity chamber was designed to be capable of intentionally adjusting pressure (ΔP) and relative humidity (φ). The points ($S1$–$S5$) signify the representative states [$S\#(\Delta P, \varphi)$] in which pressure and humidity were changed (see the Movie S2). The detailed discussion can be found in the text.

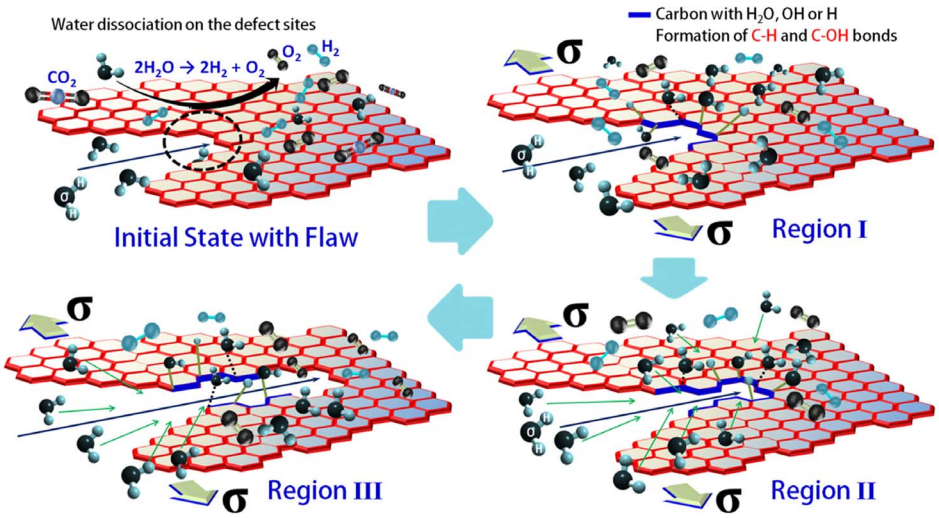

Figure 5 | Schematic illustrating the subcritical crack growth behavior of the CVD-graphene provoked from stress corrosion. The illustration summarizes the different crack velocity regions observed in the experimental ($V - K_I$) diagram in Fig. 3 with the proposed reaction between water vapor and strained C-C bonds in the graphene at the crack tip. The reactions involve, region (I): adsorption of water vapor to carbon bonds in graphene; region (II): diffusive transport of the water vapor to the graphene; region (III): electrostatic interaction between the water vapor and graphene. See the text for the details. Making reference to the literature[28,40] regarding to stress corrosion cracking, three different regions were adapted and redrawn based on our experimental data.

annealed graphene and the unannealed graphene was found that the approximate times occupied from crack initiation to catastrophic failure are different. In other words, in the case of the annealed graphene the timescale is much longer than the unannealed one. It implies that the PMMA residue could influence crack growth rate in the graphene. As mentioned above, considering the water swelling characteristics of the PMMA, the residues on the graphene is believed to function as a reservoir to furnish the graphene with water or oxygen molecules. Hence, the crack growth in the unannealed graphene with likely relatively numerous reservoirs is thought to be faster than the annealed graphene with likely few reservoirs.

Discussion

As validated so far, the polycrystalline nature of the CVD-graphene could surely allow the reactions between molecules, such as, H_2O, H_2, CO_2, NH_3, O_2 etc and carbon bonds[25–27]. The reactions and the relevant kinetics have long been interesting and intensively studied so far. Naturally, those adsorbates have an effect on the physical/chemical properties of the graphene, which have been shown to lead to new physico-chemical properties. The involved interaction kinetics can be understood via semiclassical charge transport theory[35]. Namely, in the graphene the carbon atoms are held together through sp^2-hybridized covalent bonds, while the charge is transported by hopping along π orbitals which can participate in covalent bonding with adsorbates in ambient environment. Unlike other properties, the mechanical property could be roughly understood from the viewpoint of the configuration changes caused by orbital hybridization from a planar sp^2-hybridized geometry to a distorted 3D sp^3-hybridized geometry by charge transfer. Hydrogenation (sp^3, C-H bond)[36] and folding/unzipping of graphene by the oxidation induced epoxy group (-O-) formation in graphene[37] (Fig. S15) could be typical examples. Given that water molecule dissociates into hydrogen and oxygen on defective sites of the graphene due to the enhanced reactivity (i.e. $2H_2O \rightarrow 2H_2 + O_2$)[38] and eventually leads to C-H and C-OH bonds formation[39], water molecules function as an endless hydrogen/oxygen generator. Definitely, the water molecules play a key role in stress corrosion cracking of the graphene. To be short, initially, the molecules existing in the atmosphere is thought to create bonds (such as C-H, C-OH or C-O-C) on the graphene (preferentially atomically defective sites). Those bonds induce naturally configuration changes by orbital hybridization (from 2D sp^2 geometry to 3D sp^3 geometry). Once external load is applied to the distorted graphene, the initiated or pre-existing cracks are propagated, producing fractured lines with numerous dangling bonds on the graphene. At the same time, on those defective sites created by fracturing, hydrogen and oxygen readily create new bonds or the water molecules are dissociated into hydrogen and oxygen, leaving C-H and C-OH bonds. Those yielded and pre-existing oxygen/hydrogen again create other bonds, which subsequently bring about further crack initiation/propagation triggered by the external load. These cyclic processes are thought to be repeated before reaching to catastrophic failure of the graphene.

With regard to the crack propagation path, previous researches on the subcritical crack growth in glass under varying humidity conditions[28] facilitated reasonable interpretation on those probable reactions leading to the crack propagation with three different modes. The crack velocity in the CVD-graphene gradually increases with time from $\sim 10^{-3}$ m/s to $\sim$10 m/s before reaching to catastrophic failure. When the crack propagates in the graphene, the interplays between H_2O and graphene may be repetitive and successive processes (i.e., gaseous H_2O molecules' dissociation and diffusive transport to the crack tip of the graphene, adsorption of $H_2/O_2/H_2O$ molecules by physisorption (van der Waals interaction) or chemisorption (covalent bond)), ensuing corrosive reactions between adsorbed molecules and graphene. Because the adsorption by van der Waals force in a gas phase involve negligible activation energy (typical binding energy of 10–100 meV), the physisorption will occur rapidly, thereby giving less effect on the fracture process. Contrastively, the chemisorption involves considerable activation energy (typical binding energy of 1–10 eV), thus it could control the fracture process. As a result, the control factors for the chemically enhanced fracture process are likely diffusion, chemisorption and chemical reaction. The latter two processes would depend on the stress at the crack tip, following the rate law for the chemical reaction. Thus, as described in Fig. 5, in region **I**, dissociated H_2O gas in the atmosphere reacts with carbons in the front crack tip of the graphene, resulting in reaction-rate controlled crack propagation. Accordingly, the crack velocity increases exponentially with the SIF.

In case that the liberated H_2O transports are unable to keep in step with the crack-tip propagation as SIF increases (region **II**), the crack

velocity is controlled by the H_2O diffusion rate from atmosphere to crack tip. It means that the crack velocity is not sensitive to the SIF anymore in region **II**, since H_2O diffusion to the crack tip has nothing to do with the SIF. One dimensional model for the diffusive transport of H_2O molecules to the crack tip had shown that the crack velocity in region **II** (V_{II}) has the relation, i.e. $V_{II} \sim cD/\delta n$, where c and D are the total concentration and the diffusivity of H_2O vapor, δ is diffusive boundary layer thickness, n is the order of chemical reaction (n molecules of water are required to break the C-C bond in the graphene, nH_2O + Bond → Broken Bond)[40]. In case of 3D materials with m atomic layers, the functional relation between V_{II} and m could be described as $V_{II} \sim cD/\delta nm$ (Fig. S16). Hence, the crack velocity of 3D ($m > 1$) materials in region **II** should be much slower than the velocity of 2D ($m = 1$) materials. In addition, unlike 3D materials having a cracked surface, the monolayer graphene has not a cracked surface but a cracked line. It means that dissociated water molecules in air can easily access and break a few carbon bonds in the crack line of the graphene, thereby leading to faster crack velocity. Indeed, as summarized in Table S4, V_{II} of the graphene (from $\sim 10^{-2}$ to $\sim 10^{-1}$ m/s) is noticeably faster than the V_{II} of the 3D bulk materials (e.g. V_{II} of $Al_2O_3 \approx 10^{-4}$ m/s). Accordingly, the velocity of this intermediate branch, region **II**, depends on the diffusion rate of the corrosive H_2O vapor into the crack tip and the number of the bonds present in the crack tip.

Contrary to regions **I** and **II**, the crack growth in region **III** showed strong dependence on the SIF. As can be seen in Fig. 3, with increasing SIF, the crack velocity accelerates rapidly till finally reaching the allowed SIF, i.e. fracture toughness value (K_{Ic}). Speculating the phenomenon occurring in this region, it is believed that, owing to the rapid crack velocity, presumably the H_2O molecules are unable to reach the crack tip, as depicted in region **III** of Fig. 5. The most probable factors governing the fracture process in region **III** was reported to be electrostatic interactions between the medium fluid and the highly strained bonds at the crack tip[28]. Considering this report, in our case, the dielectric constant of water and the stretching of C-C bonds in the CVD-graphene by applied stress are thought to be the main parameters responsible for the subcritical crack growth behavior by the stress corrosion cracking. As another surmisable reason, at a sufficiently large crack velocity, the increase of the thermal and inertial energy around the crack tip induced by crack growth is considered to accelerate the bond breakage in proportion to SIF regardless of water diffusion in region **III**.

To conclude, the monolayer CVD-graphene exposed to the room condition turned out to undergo subcritical crack growth due to the stress corrosion which is enabled from the susceptibility of the CVD-graphene to various adsorbates, such as water vapor. Nevertheless, fracture toughness of the CVD-graphene appeared to be exceptionally high (10.7 ± 3.3 MPa $m^{1/2}$), which implies that the CVD-graphene could be an ideal candidate as a structural material despite of environmental susceptibility. It was validated that the PMMA residues have a minor effect on general fracture behavior of the graphene, although it functions as water reservoir to accelerate stress corrosion cracking of the graphene or crack arrestors. Furthermore, the propagation of cracks on the graphene appeared to be able to be reasonably tamed by adjusting applied humidity and stress. Our experiments showed that time dependent non-continuum fracture behaviors occurring in 2D mono-atomic structures can be macroscopically well visualized and characterized. It is highly anticipated that the measurements reported here provide a significant first step forward in disclosing the hidden physics, particularly solid mechanics, of ideal 2D structures.

Methods

Graphene synthesis using CVD. Single-layer graphene was synthesized using chemical vapor deposition (CVD). Copper foil (99.8% purity and 25 μm thick, No.13382, Alfa Aesar) was used as catalyst. The copper foil was loaded into a 2 inch quartz tube in a CVD furnace setup and then purged with Ar flow (500 sccm) for 10 min. Then, copper was annealed and reduced in a CVD furnace at 850°C for 40 min in low pressure (~700 mtorr) with Ar (50 sccm)/H_2 (20 sccm) mixture flow. Subsequently, in low pressure, growth was performed at 1000°C for 10 min with the mixture flow of CH_4 : H_2 (30 sccm : 30 sccm). In order to induce slow cooling of the sample, the CVD furnace was maintained without opening the lid until the inside temperature reaches 700°C. Then, the sample was rapidly cooled down by opening the lid of the furnace.

Preparation of the suspended graphene membrane. In order to prepare suspended membrane, as-grown CVD-graphene was transferred onto the target Si substrate with a cylindrical circular hole, using a PMMA (polymethylmethacrylate) based transfer method (Figure S1). Namely, a thin film of PMMA (PMMA 950 A4, MicroChem) was spin-coated (~200 nm thick) on the surface of the graphene/copper sample and then the copper was etched away using ammonium persulfate (APS) solution. This left a floating PMMA/graphene sample on the APS solution surface, which was scooped with a piece of Si-wafer and transferred to a flat beaker of deionized water to rinse off any impurity and residue of APS. These rinsing processes were repeated several times with fresh deionized water. Then, the floating sample was scooped up on the Si substrate with a cylindrical circular hole, followed by drying in air. Finally, the PMMA of the sample was dipped into a flat beaker filled with acetone on a hot plate for over one hour. The temperature of the hot plate was maintained to be 70°C and the acetone was continuously stirred with a magnetic stirring bar. These etching processes were repeated several times with fresh acetone, followed by drying overnight in room condition. The prepared graphene membranes were examined using an optical microscope (Eclipse LV-100D, Nikon) whether or not the membranes burst, and subsequently kept in a desiccator before performing experiments. The cylindrical circular hole on Si-wafer [500 μm thickness with SiO_2 (300 nm) layer] was fabricated by photolithography and reactive ion etching.

Annealing of graphene membranes. In order to minimize the PMMA residues on the prepared graphene membranes suspended on cylindrical holes, the graphene membranes were gently transferred to a tubular furnace. The membranes were thermally annealed at 250°C and 350°C, respectively, for two hours in low pressure (~1 torr) with Ar flow (500 sccm). After thermal annealing, under the optical microscope, firstly the graphene membranes were once more examined whether the membranes were alive. Subsequent characterizations were performed one by one.

Characterization. The morphologies and surface structures of the suspended CVD-graphene samples were examined by scanning electron microscope (SEM) (FEI, Nova nanoSEM 200) and optical microscope (Eclipse LV-100D, Nikon). Micro Raman spectroscopy measurement (inVia Raman Microscope, Renishaw) was employed to ensure that the resulting suspended CVD-graphene membranes were predominantly monolayer graphene. The Raman spectrometer was equipped with 514 nm laser line and an objective (×50). To avoid local heating effects, the laser power density was kept below 100 μW/μm^2. The backscattered Raman light was diffracted by an 1800 g/mm grating and detected by a charged coupled device camera. Topographic features were evaluated using contact mode AFM measurement (NanoWizard® II, JPK Instrument).

Observation of fracture behavior of CVD-graphene. For this experiment, over 1400 samples (graphene/SiO_2/Si) with various sizes were initially prepared. Before performing the experiment, the suspended graphene membrane sample on Si substrate was carefully examined one by one with the optical microscope in order to confirm whether the graphene is safely suspended on Si substrate because the membrane was often ripped due to the unavoidable mechanical stress developing during wet etching and drying in air. Among 1400 samples, about 400 samples with various sizes were found to be successfully suspended on the silicon substrate without breakup of the graphene membrane. However, in this experiment, an optical microscope for observation of graphene fracture was used. The limited resolution of the optical microscope forced us to prepare large sample which is suitable for further observation. Although samples with diameter of 10 ~ 20 μm were relatively easy to prepare, those samples were too small to further investigate using an optical microscope. As another problem, we witnessed that although PMMA based wet transfer method facilitates increase of the graphene membrane size, the PMMA method results in PMMA residues (island shaped) on the prepared graphene membrane. As an alternative, PDMS (polydimethylsiloxane) based transfer method was tried for a while. Although the residue problem was able to get resolved, the maximum achievable size of graphene membrane using the PDMS transfer method was at the most few micrometers in diameter. As a final choice, thermal annealing was performed and marked reduction of PMMA residue was observed. However, most of large samples were observed to burst due to thermal stress during annealing. To the best of our ability, the maximum achievable sizes of the graphene membranes by annealing at 250°C and 350°C were 20 μm and 10 μm, respectively. In case of membrane with a diameter of 10 μm, the size was not large enough to further investigate using the optical microscope. Thus, in order to observe fracture behavior of the annealed graphene membrane, samples annealed at 250°C were used.

Unannealed graphene membrane. Using the experimental setup schematically shown in Figure 2a, the fracturing behavior of the suspended CVD-graphene membrane under quasistatic pressure was observed in the conditions of T = 20°C and relative humidity = 35%. Per each sample, bulge test together with detailed structural analyses were carefully carried out under nearly identical environmental

conditions. In order to precisely capture the moment of fracturing, gradually increasing the pressure difference (P_{atm} - P_i) at a rate of 0.1 kPa, we constantly monitored the shape change of the pressurized suspended graphene membrane in real time. We observed that our graphene membranes start to fracture at the gauge pressure of 1.5 ~ 36 kPa. At the same time, the fracturing behavior was recorded at the shutter speed of 500 fps with the frame size of 512 × 512 pixels using a high speed camera (×100, Fastcam 1024 PCI, Photron). To capture whole processes of fracture (i.e., from crack initiation to catastrophic failure) with good resolution was hard tasks. Sometimes, we obtained a just partially recorded movie because crack initiation/propagation was finished in a wrinkle. In some membranes, the length of the whole fracture process exceeded maximum recording capacity of high speed camera. In the other cases, the image resolution was rather poor to precisely recognize crack initiation and propagation, although the whole fracture process was successfully recorded. These experimental history and obstacles forced us to prepare lots of samples. Over around 80% of those samples were not able to be used in the experiment due to the inappropriate sample size or burst during the sample preparation or the experiment without giving meaningful data. Only some of those remaining samples provided us data which at least deserved further consideration. For this reason, among 1400 samples, fracture behaviors of only 20 samples were successfully recorded. Among the obtained data set, some of data were again filtered carefully for the publication. Through these processes, only 7 dataset were finally selected. (Table S1). From the recorded *.tif formatted raw image files, we produced a representative motion picture showing the fracturing behavior of the CVD-graphene (diameter: 90 μm, Fig. S3, see Movie S1). The crack length variations per 2 ms in the selected datasets were carefully measured one by one making use of a built-in software in the optical microscope (see the details in Fig. 2b and Fig. S4). Because the stress intensity factor is dependent on not only the size but also the shape of the flaw, one had to pay close attention. The measured data were over 3000 points per each dataset. Because all the data were not able to be included in the single graph of the crack length versus the time, data per 60 ms were selectively used to make a graph. In order to obtain the crack growth rate versus time diagram, from the discrete data in the crack length versus the time diagram, the numerical differentiation was performed by averaging the slopes of two adjacent points using ORIGIN® 8.0 software. Further graphical tasks were performed with ORIGIN® 8.0. As an editing tool for motion picture, Adobe Premiere CS 4 software was used.

Annealed graphene membrane. As depicted in the inset of Fig. 4b, a humidity chamber was designed, in which pressure (ΔP) and relative humidity (φ) were able to be intentionally adjusted. Instead of the unannealed CVD-graphene, the annealed CVD-graphene (250°C, 2 h) with negligible amount of PMMA residues was used in bulge test. As described in the profile of pressure (ΔP)/humidity (φ) vs time (t) in Fig. 4b and Figs. S13–S14, pressure and humidity were adjusted and at the same time all images were sequentially recorded with CCD (charge coupled device) camera(×100) at a rate of 37 fps (DS-Fi2, Nikon). Because the duration of the fracture process took exceeded the recording capacity of our high speed camera, CCD camera with longer recoding limit was employed for the observation and recording. From the recorded raw image files (*.tif), we produced a representative motion picture showing the fracturing behavior of the CVD-graphene (diameter: 20 μm, see Movies S2–S4). Motion pictures were edited with Adobe Premiere CS 4 software.

Investigation of survival ratio of the CVD graphene under different humidity conditions. Dozens of the unannealed CVD-graphene membrane samples suspended on a hole were firstly prepared, respectively. The relative humidity of the specially designed isothermal-isohumidity chamber was regulated before experiment. Under the relative humidity of 95%, or 15%, the samples were kept, respectively. Every hour, the samples were taken out and examined using the optical microscope whether the membranes are broken or not. By counting the number of the broken/unbroken samples, the survival ratios were calculated.

1. Griffith, A. A. The phenomena of rupture and flow in solids. *Philos. Trans. R. Soc. London, Ser. A* **221**, 163–198 (1921).
2. Irwin, G. R. Analysis of stresses and strains near the end of a crack traversing a plate. *J. Appl. Mech.* **24**, 361–364 (1957).
3. Novoselov, K. S. *et al.* Electric field effect in atomically thin carbon films. *Science* **306**, 666–669 (2004).
4. Geim, A. K. Graphene: status and prospects. *Science* **324**, 1530–1534 (2009).
5. Novoselov, K. S. *et al.* A roadmap for graphene. *Nature* **490**, 192–200 (2012).
6. Omeltchenko, A., Yu, J., Kalia, R. K. & Vashishta, P. Crack front propagation and fracture in a graphite sheet: a molecular-dynamics study on parallel computers. *Phy. Rev. Lett.* **78**, 2148–2151 (1997).
7. Grantab, R., Shenoy, V. B. & Ruoff, R. S. Anomalous strength characteristics of tilt grain boundaries in graphene. *Science* **330**, 946–948 (2010).
8. Xu, M., Tabarraei, A., Paci, J. T., Oswald, J. & Belytschko, T. A coupled quantum/continuum mechanics study of graphene fracture. *Int. J. Fract.* **173**, 163–173 (2012).
9. Zhang, T., Li, X., Kadkhodaei, S. & Gao, H. Flaw insensitive fracture in nanocrystalline graphene. *Nano Lett.* **12**, 4605–4610 (2012).
10. Zhang, J., Zhao, J. & Lu, J. Intrinsic strength and failure behaviors of graphene grain boundaries. *ACS Nano* **6**, 2704–2711 (2012).
11. Kotakoski, J. & Meyer, J. C. Mechanical properties of polycrystalline graphene based on a realistic atomistic model. *Phys. Rev. B* **85**, 195477 (2012).
12. Wei, Y. *et al.* The nature of strength enhancement and weakening by pentagon-heptagon defects in graphene. *Nature Mater.* **11**, 759–763 (2012).
13. Lee, C., Wei, X., Kysar, J. W. & Hone, J. Measurement of the elastic properties and intrinsic strength of monolayer graphene. *Science* **321**, 385–388 (2008).
14. Ruiz-Vargas, C. S. *et al.* Softened elastics response and unzipping in chemical vapor deposition graphene membranes. *Nano Lett.* **11**, 2259–2263 (2011).
15. Huang, P. Y. *et al.* Grains and grain boundaries in single-layer graphene atomic patchwork quilts. *Nature* **469**, 389–393 (2011).
16. Kim, K. *et al.* Ripping graphene: preferred directions. *Nano Lett.* **12**, 293–297 (2012).
17. Kim, K. *et al.* Multiply folded graphene. *Phys. Rev. B.* **83**, 245433 (2011).
18. Li, X., Cai, W., Colombo, L. & Ruoff, R. S. Evolution of graphene growth on Ni and Cu by carbon isotope labeling. *Nano Lett.* **9**, 4268–4272 (2009).
19. Nie, S., Wofford, J. M., Bartelt, N. C., Dubon, O. D. & McCarty, K. F. Origin of the mosaicity in graphene grown on Cu(111). *Phys. Rev. B.* **84**, 155425 (2011).
20. Ferrari, A. C. *et al.* Raman spectrum of graphene and graphene layers. *Phys. Rev. Lett.* **97**, 187401 (2006).
21. Casiraghi, C., Pisana, S., Novoselov, K. S., Geim, A. K. & Ferrari, A. C. Raman fingerprint of charged impurities in graphene. *Appl. Phys. Lett.* **91**, 233108 (2007).
22. Das, A. *et al.* Monitoring dopants by Raman scattering in an electrochemically top-gated graphene transistor. *Nat. Nanotechnol.* **3**, 210–215 (2008).
23. Metzger, C. *et al.* Biaxial strain in graphene adhered to shallow depressions. *Nano Lett.* **10**, 6–10 (2010).
24. Sharon, E., Gross, S. P. & Fineberg, J. Local crack branching as a mechanism for instability in dynamic fracture. *Phy. Rev. Lett.* **74**, 5096–5099 (1995).
25. Salehi-Khojin, A. *et al.* Polycrystalline graphene ribbons as chemiresistors. *Adv. Mater.* **24**, 53–57 (2012).
26. Schedin, F. *et al.* Detection of individual gas molecules adsorbed on graphene. *Nature Mater.* **6**, 652–655 (2007).
27. Leenaerts, O., Partoens, B. & Peeters, F. M. Adsorption of H_2O, NH_3, CO, NO_2, and NO on graphene: A first-principles study. *Phys. Rev. B* **77**, 125416 (2008).
28. Wiederhorn, S. M., Freiman, S. W., Fuller Jr, E. R. & Simmons, C. J. Effects of water and other dielectrics on crack growth. *J. Mater. Sci.* **17**, 3460–3478 (1982).
29. Lim, L. C. & Watanabe, T. Grain boundary character distribution controlled toughness of polycrystals-A two-dimensional model. *Scripta Metall.* **23**, 489–494 (1989).
30. Watanabe, T. Approach to grain boundary design for strong and ductile polycrystals. *Res. Mechanica* **11**, 47–84 (1984).
31. Wiederhorn, S. M. Brittle fracture and toughening mechanisms in ceramics. *Ann. Rev. Mater. Sci.* **14**, 373–403 (1984).
32. Mohiuddin, T. M. G. *et al.* Uniaxial strain in graphene by Raman spectroscopy: G peak splitting, Grüneisen parameters, and sample orientation. *Phys. Rev. B* **79**, 205433 (2009).
33. Suk, J. W. *et al.* Enhancement of the electrical properties of graphene grown by chemical vapor deposition via controlling the effects of polymer residue. *Nano Lett.* **13**, 1462–1467 (2013).
34. Ashby, M. F. & Bréchet, Y. J. M. Designing hybrid materials. *Acta Materialia* **51**, 5801–5821 (2003).
35. Lherbier, A. *et al.* Charge transport in chemically doped 2D graphene. *Phys. Rev. Lett.* **101**, 036808 (2008).
36. Topsakal, M., Cahangirov, S. & Ciraci, S. The response of mechanical and electronic properties of graphene to the elastic strain. *Appl. Phys. Lett.* **96**, 091912 (2010).
37. Schniepp, H. C. *et al.* Functionalized single graphene sheets derived from splitting graphite oxide. *J. Phys. Chem. B* **110**, 8535–8539 (2006).
38. Kosttov, M. K., Santiso, E. E., George, A. M., Gubbins, K. E. & Buongiorno Nardelli, M. Dissociation of water on defective carbon substrate. *Phy. Rev. Lett.* **95**, 136105 (2005).
39. Poitano, A., Marino, A. R., Formoso, V. & Chiarello, G. Water adsorption on graphene/Pt(111) at room temperature: a vibrational investigation. *AIP Adv.* **1**, 042130 (2011).
40. Wiederhorn, S. M. Influence of water vapor on crack propagation in soda-lime glass. *J. Amer. Ceram. Soc.* **59**, 407–414 (1967).

Acknowledgments

This research was supported by the Industrial Core Technology Development Programs of the Korean Ministry of Knowledge Economy (grant 10033309), National Platform Technology Programs of the Korean Ministry of Knowledge Economy (grant 10034751), the Center for Nanoscale Mechatronics and Manufacturing, one of the 21st Century Frontier Research Programs of the Korean Ministry of Education, Science and Technology, and Innovative Research Programs of Korea Institute of Machinery and Materials.

Author contributions

S.-M.L. conceived the project and wrote the manuscript. Y.H. and C.L. and designed the study and performed experiments. S.-M.K., K.-S.K., B.J. and S.-K. L. contributed to experiments, data analysis and discussions. J.-H.K., H.-J.L., S.-S.K. and J.-H.A. discussed the results and coached the direction of the project.

Additional information

Supplementary information accompanies this paper at http://www.nature.com/scientificreports

Competing financial interests: The authors declare no competing financial interests.

How to cite this article: Hwangbo, Y. *et al*. Fracture Characteristics of Monolayer CVD-Graphene. *Sci. Rep.* **4**, 4439; DOI:10.1038/srep04439 (2014).